HELZ promotes R loop resolution to facilitate DNA double-strand break repair by homologous recombination

Ramona Haji-Seyed-Javadi[1], Allyson E. Koyen[1], Sandip K. Rath[1], Matthew Z. Madden[1], Yingzi Hou[2], Boying S. Song[1], Anna M. Kenney[3], Li Lan[4], Bing Yao[2], and David S. Yu[1*]

[1] Department of Radiation Oncology and Winship Cancer Institute, Emory University School of Medicine, Atlanta, GA 30322, USA
[2] Department of Human Genetics, Emory University School of Medicine, Atlanta, GA 30322, USA
[3] Department of Pediatrics and Winship Cancer Institute, Emory University School of Medicine, Atlanta, GA 30322, USA
[4] Department of Molecular Genetics and Microbiology, Duke University School of Medicine, Durham, NC 27710, USA

*Correspondence: dsyu@emory.edu

[*]Corresponding Author:
David S. Yu, M.D., Ph.D.
Department of Radiation Oncology
Emory University School of Medicine
1365 Clifton Rd NE, C3008
Phone: 404-778-1758, Fax: 404-778-5520
e-mail: dsyu@emory.edu

Abstract

R loops are RNA-DNA hybrid containing structures involved in diverse cellular processes, including DNA double-strand break (DSB) repair. R loop homeostasis involving the formation and resolution of R loops is critical for DSB repair, and its dysregulation leads to genome instability. Here we show that the HELZ helicase promotes R loop resolution to facilitate DSB repair by homologous recombination (HR). HELZ depletion causes hypersensitivity to DSB-inducing agents, and HELZ localizes and binds to DSBs. HELZ depletion further leads to genomic instability in a R loop dependent manner and the accumulation of R loops globally and at DSBs. HELZ binds to R loops in response to DSBs and promotes their resolution, thereby facilitating HR to promote genome integrity. Our findings thus define a role for HELZ in promoting the resolution of R loops critical for DSB repair by HR.

Introduction

R loops are nucleic acids structures consisting of a RNA-DNA hybrid with a displaced single-stranded DNA (ssDNA). R loops are prevalent, occupying about 5% of the human genome[1], and can form in multiple contexts, most frequently when a nascent RNA transcript hybridizes with the template ssDNA[2,3]. R loops are involved in diverse cellular processes, including transcription, DNA replication, DNA repair, telomere homeostasis, histone modification, and immunoglobulin class switch recombination[2-8]. While R loops play an important role in many physiological functions, dysregulation of R loop homeostasis resulting in unresolved or excessive accumulation of R loops can lead to DNA damage and genomic instability[2-8]. Dysregulation of R loop is also associated with number of diseases, including autoimmune disease, neurological disorders, and cancer[9]. Thus, the formation, resolution, and prevention of R loops must be tightly regulated.

DNA double-strand breaks (DSB) are highly cytotoxic lesions which must be repaired in order to preserve genome integrity[10-12]. DSBs are repaired predominantly by two major pathways: homologous recombination (HR), which involves repair using a sister chromatid as a template and is error-free, and non-homologous end joining (NHEJ), which involves direct ligation of broken DNA ends and is error-prone. R loops have been reported at DSB sites[13,14] and can both promote and impair DSB repair[15]. However, the mechanisms by which R loops are resolved to promote DSB repair are still not well understood.

Helicase with Zinc Finger (HELZ) is a member of the superfamily I (SF1) class of RNA helicases that alter the conformation of RNA by unwinding double-stranded regions. Very little is known about HELZ with only two references characterizing HELZ in PubMed. HELZ contains an amino-terminal C3H1-type zinc finger motif, a Walker A motif conferring ATP binding, a Walker B DEAA [Asp, Glu, Ala, Ala] box helicase motif, and an unstructured carboxyl-terminal region

with a conserved poly(A) binding protein interacting motif 2 (PAM2). HELZ promotes cell proliferation, translation initiation, and ribosomal protein 6 phosphorylation[16] and interacts with the carbon catabolite repressor 4-negative on TATA box (CCR4-NOT) deadenylase complex and causes decay of bound mRNAs[17]. HELZ has not previously been linked to R loops or DNA repair.

In this study, we define a role for HELZ in promoting R loop resolution to facilitate DSB repair by HR.

Results

HELZ depletion causes hypersensitivity to DSB-inducing agents and HELZ localizes to DSBs

We identified HELZ in a siRNA screen of a library of "nuclear enzymes" that mediate etoposide resistance in H128 small cell lung cancer cells (SCLC) cells (manuscript being submitted separately for characterization of another gene that was the strongest positive hit). We validated that HELZ depletion by multiple siRNA causes etoposide hypersensitivity in H128 and U2OS osteosarcoma cells (Fig. 1a and Supplementary Fig. S1a), suggesting that the phenotype is not cell type specific. We generated a custom rabbit polyclonal anti-HELZ antibody and confirmed HELZ knockdown in these cells (Fig. 1c and Supplementary Fig. S1c). This antibody also recognizes overexpressed GFP/RFP-HELZ (Fig. 3d and 5c) thus confirming the specificity of the antibody for both endogenous and overexpressed HELZ. HELZ depletion also caused hypersensitivity to ionizing radiation (IR) and camptothecin (CPT) (Fig. 1b and Supplementary Fig. S1b), suggesting that HELZ responds generally to DNA double-strand breaks (DSB).

HELZ localizes and binds to DSBs

To determine if HELZ localizes to DSBs, we induced DSBs using mCherry-LacI-Fok1 endonuclease in U2OS reporter cells integrated with lac operator repeats[18]. GFP-HELZ co-localized with Fok1-induced DSBs that were also marked by γH2AX (Fig. 1d), suggesting that HELZ localizes to DSBs. A proximity ligation assay (PLA) validated the proximity of HELZ with γH2AX following etoposide treatment (Fig. 1e-f). To determine if HELZ binds to endogenous DSBs, we performed chromatin IP (ChIP) with quantitative PCR (qPCR) using U2OS DIvA (DSB Inducible via AsiSI) cells, in which 4-hydroxytamoxifen (4-OHT) treatment triggers nuclear localization of AsiSI to induce approximately 150 sequence-specific DSBs, dispersed across the genome[19]. HELZ showed enriched accumulation to HR1 and HR2 prone DSB repair sites after 4-OHT treatment (Fig. 1g-h), suggesting that HELZ binds to DSBs. We found no evidence for a change in HELZ protein levels or nuclear-cytoplasmic localization by biochemical fractionation following etoposide treatment (Supplementary Fig. S1d-e).

HELZ depletion causes genomic instability via R loop accumulation

To determine if HELZ depletion leads to genomic instability, we examined for accumulation of spontaneous γH2AX. HELZ depletion led to an increase in γH2AX in U2OS, RPE-1 nontumorigenic hTERT immortalized retinal pigment epithelial cells, and HeLa cervical cancer cells (Fig. 2a-b and Supplementary Fig. S2a-d). HELZ depletion also led to an increased percentage of U2OS cells with micronuclei compared with a NT control (Fig. 2c-d). Moreover, HELZ depletion or knockout (KO) by CRISPR/Cas9 in U2OS cells and HELZ depletion in RPE-1 and HeLa cells led to an increase in 53BP1 nuclear bodies (Fig. 2e-g and Supplementary Fig. S2e-h)). Interestingly, the increase in 53BP1 nuclear bodies resulting from HELZ depletion was rescued by overexpression of mCherry-Ribonuclease (RNase) H1, which catalyzes the cleavage

of RNA in DNA-RNA hybrids (Fig. 2h-i), suggesting that HELZ depletion causes genomic instability via R loop accumulation.

HELZ prevents accumulation of R loops through its helicase activity

Several members of the DEAD box family of RNA helicases are involved in R-loop homeostasis [20]. Given that HELZ is reported as a putative RNA helicase[REF], we determined whether HELZ depletion leads to an increase in R loops as determined by immunofluorescence microscopy using the S9.6 monoclonal antibody. An increase in S9.6 signal intensity was observed with HELZ depletion compared with a NT control in U2OS cells, which was rescued by RNaseH treatment (Fig. 3a-b), demonstrating specificity of HELZ in preventing accumulation of endogenous R loops. We validated that HELZ depletion or etoposide treatment leads to an increase in S9.6 signal in HCT-116 colorectal cells by slot blot analysis, although no further increase in S9.6 signal was observed with combined HELZ depletion and etoposide treatment (Fig. 3c-d), [suggesting that HELZ may play a role in preventing etoposide-induced R loops?]. Overexpression of GFP-HELZ wild-type (WT) but not K674N, a mutation in the Walker A motif, which abolishes ATPase activity in DEAD box helicases[21] (Supplementary Fig. S3), alleviated the induction of S9.6 signal intensity of HELZ depletion (Fig. 3c-d), suggesting that HELZ prevents accumulation of R loops in cells through its helicase activity. To determine if HELZ interacts with R loops, we performed DNA-RNA immunoprecipitation (DRIP) analysis using the S9.6 antibody, which showed an interaction of HELZ with R loops that was increased after treatment of cells with etoposide or CPT and abolished with RNase H or RNase A treatment (Fig. 3e), suggesting that HELZ binds to R loops and that this interaction increases in response to DSBs. Consistently, both HELZ and S9.6 showed an enriched accumulation to HR1 prone DSBs in DIvA cells after

induction of DSBs (Fig. 3f). To determine whether HELZ prevents accumulation of R loops at DSBs, we performed PLA with γH2AX and S9.6 following HELZ depletion. A significant increase in γH2AX and S9.6 PLA foci following HELZ depletion was observed (Fig. 3g-h), suggesting that HELZ prevents the accumulation of R loops at DSBs.

HELZ depletion causes global accumulation of R loops

To determine the global impact of HELZ deficiency on R loops, we performed DRIP sequencing (DRIP-seq) analysis following IP of DNA-RNA hybrids with the S9.6 anitbody in U2OS cells silenced for HELZ. DRIP-seq profiling revealed 84,618 R-loop peaks that overlapped with 14,121 annotated genes (RefSeq, hg38) in siNT cells and 91,172 R-loop peaks that overlapped with 14,231 annotated genes in siHELZ cells (Supplementary Fig. S4a-b). Most of the R-loop-positive genes (12,845) were common to both cells (Supplementary Fig. S4b). We plotted R-loop read counts across all R-loop peaks identified in both cells and found that R-loops were upregulated upon HELZ depletion (Fig. 4a, $p = 1.36x10^{-7}$) and was decreased in cells treated with RNase H. A substantial portion of R-loops were located in gene body regions (71%, including exons and introns) which may suggest an active transcription of the genes (Supplementary Fig. S4a). We then plotted R-loop read counts across defined human RefSeq (hg38) genes and found that R-loops in both cells were enriched across the genes compared to RNase H-treated samples (Fig. 4b). HELZ depletion showed a global R-loop accumulation in the genomic regions (Fig. 4b, $p = 1.97x10^{-10}$). Using DESeq2, we identified 3,793 regions that accumulated R-loops significantly upon HELZ knockdown, and 3,357 regions that showed depleted R-loops (Fig. 4c, false discovery rate (FDR) < 0.05, $\log_2$(Fold change) > 1). The R-loop read count plotting confirmed an increase of R-loops across the accumulated R-loop regions (Fig. 4d, $p = 1.70x10^{-18}$) and a decrease of R-

loops across the depleted R-loop regions (Fig. 4e, $p = 7.91x10^{-22}$). In general, differential R-loops were enriched in 3'UTR, 5'UTR, exon, intron, promoter, and transcription termination sites (TTS), compared to expected values (Fig. 4f, Supplementary Fig. S4c).

HELZ promotes homologous recombination by preventing accumulation of R loops at DSBs

PARP inhibitor sensitivity is associated with impairment in HR [22]. Indeed, similar to BRCA2, HELZ depletion in U2OS cells caused hypersensitivity to ABT888 (Veliparib), a PARP inhibitor (Fig. 5a). To determine directly if HELZ functions in HR, we examined HELZ depletion in 293T and U2OS cells integrated with the direct repeat (DR)-GFP HR reporter substrate in which expression of the rare cutting endonuclease I-SceI generates a DSB which when repaired by HR restores GFP expression. Similar to CtIP, HELZ depletion impaired HR (Fig. 5b-c and Supplementary Fig. S5a), which was alleviated by expression of RFP-HELZ WT but not K674N (Fig. 5b-c), suggesting that HELZ helicase activity promotes HR. We observed no significant decrease in cells in S and G2 phase following HELZ depletion, suggesting that the impairment in HR is not an indirect effect of cell cycle change (Supplementary Fig. S5c). To determine whether HELZ functions in non-homologous end joining (NHEJ), we examined HELZ depletion in 293 cells integrated with the EJ7 classical NHEJ (c-NHEJ) reporter. In contrast to its impact on HR, HELZ depletion caused an increase in c-NHEJ (Fig. 5d-e), suggesting that HELZ may play a role in determining DSB repair pathway choice by HR vs c-NHEJ. Consistent with our reporter data, HELZ depletion in U2OS cells caused an impairment in IR-induced RAD51 foci (Fig. 5f-g and Supplementary Fig. S5d-e) and an increase in IR-induced RIF1 foci (Fig. 5h-i). Interestingly, the impairment in IR-induced RAD51 foci resulting from HELZ depletion was alleviated by treatment

of cells with RNAse H and RNase A (Fig. 5f-g), suggesting that HELZ promotes HR by preventing accumulation of R loops at DSBs.

Discussion:

Our findings reveal a role for HELZ in the resolution of R loops to promote DSB repair by HR. These findings identify HELZ as a critical regulator of R loop homeostasis by resolving R loops, establish HELZ as an important factor in promoting DSB repair by HR, and provide a mechanistic link between the removal of R loops and promotion of HR via HELZ to promote genome integrity. In this regard, we found that HELZ depletion causes hypersensitivity to DSB-inducing agents IR and etoposide and HELZ localizes and binds to DSBs. HELZ depletion further leads to the spontaneous accumulation of γH2AX and 53BP1 nuclear bodies, which can be rescued by RNase H1 expression, suggesting that HELZ prevents genomic instability in a R loop-dependent manner. Moreover, HELZ binds to R loops in response to etoposide and CPT treatment and prevents their accumulation in a helicase activity-dependent manner, globally, and in response to DSBs. HELZ helicase activity furthermore promotes HR, and the impairment in IR-induced RAD51 foci from HELZ depletion is alleviated by RNase H treatment, suggesting that HELZ promotes HR by preventing the accumulation of R loops at DSBs. Thus, our findings are consistent with a model in which in response to DSBs, HELZ localizes, binds, and resolves unscheduled harmful R loops at DSBs to facilitate HR and promote genome integrity.

HELZ has previously been reported to promote cell proliferation, translation initiation, and ribosomal protein 6 phosphorylation[16] and regulates the stability and translation of mRNA via its interaction with mRNA decay factors in the cytoplasm[17]. We now report that HELZ has an important role in promoting genome stability by resolving R loops to facilitate DSB repair by HR.

In addition, our DRIP-seq analysis also indicate an enrichment of R loops at transcription start and termination sites with HELZ depletion, suggesting that HELZ also helps to resolve harmful co-transcriptional R loop structures.

It has been reported that the accumulation of R loops around DSBs competes with RAD51 localization and binding to DSBs[23]. Consistent with these data, we found that the impairment in IR-induced RAD51 foci from HELZ depletion was alleviated by RNase H and RNase A treatment, suggesting a role for R loops in impairing HR and that HELZ resolves R loops to facilitate HR. In addition, as we found that HELZ depletion leads to an increase in NHEJ as determined using a direct EJ7-NHEJ reporter assay and IR-induced RIF1 foci, these data suggest that HELZ's role in resolving R loops may play a role in determining DSB repair pathway choice between HR and NHEJ.

A number of helicases, including Senataxin[24-26], AQR[27], UPF1[28], PIF1[29], WRN[30], BLM[31], RTEL1[32], FANCM[33-35]; POLQ[36], ATRX[37], SMARCAL1[33], ZRANB3[33], DDX1[38-40], DDX5[41], DDX17[42], DDX18[43], DDX19[44], DDX21[45,46], DDX23, UAP56/DDX39B[47], DDX41[48,49], DDX47[50] and DHX9[51-54] have been reported to be involved in R loop homeostasis with Senataxin[55,56], AQR[57], BLM[58], DHX9[52,59], DDX1[38,39], DDX5[60], DDX17[42], DDX18[43], and UPF1[28] involved in facilitating the repair of DSBs. How HELZ may function with these helicases in resolving R loop homeostasis to facilitate DSB repair is unclear. It is possible that HELZ may act on specific types of R loop structures or sites or act in a temporal manner potentially in collaboration with other helicases.

Given that HELZ depletion sensitizes cancer cells to IR, PARP inhibitor, and other DSB-inducing agents, our findings provide rationale for targeting the helicase activity of HELZ as an adjunct to DSB-inducing agents.

Methods

Cell lines. Human SCLC line NCI-H128 was provide by the laboratory of Dr. Taofeek Owonikoko and grown in RPMI 1640 (Gibco) with 7.5% FBS. HEK293T, HCT116, HeLa and U20S mammalian cell lines were purchased from American Type Culture Collection (ATCC, Manassas, VA). U20S-235 mCherry-LacI-Fok1 cell line were provided by Dr. Roger Greenberg. and U20S-DR-GFP, HEK293-DR-GFP and HEK293-EJ7-GFP cell lines were obtained from Dr. Jeremy Stark. AsiSI-ER-U2OS (DIvA-DSB inducible via AsiSI) cells were provided by Dr. Gaëlle Legube. All cell lines were grown in DMEM (Gibco) antibiotic-free media supplemented with 7.5% FBS. U20S-235 was additionally cultured in 2 μg/mL puromycin and 100 μg/mL hygromycin. DIvA cells were additionally cultured in 1 μg/mL puromycin. All cell lines were grown at 37 °C under humidified conditions with 5% CO2 and 95% air.

Cell viability assay. Cell viability assays were performed as previously described [6]. Cells were seeded in 96- well plates at the appropriate density (H128: 10,000 cells/well H146: 20,000 cells/well) and were treated with varying doses of etoposide (10-25 μM). For UV treatment, cells were irradiated with the indicated dose of UV prior to seeding. After treatment, cells were grown in 96-well plates for 72 hours and then treated with Resazurin reagent at a final concentration of 1X in media. Cells were then incubated at 37°C for 3 hours. The Resazurin signal was then read as fluorescence (excitation wavelength: 544 nm, emission wavelength:590 nm) on a Synergy H1 microplate reader (BioTek) in conjunction with Gen5 Microplate Reader Software (BioTek). Percent cell viability was quantified relative to the Resazurin signal in the untreated group,

including subtracting the background the Resazurin signal for wells with no cells and media with Resazurin only.

Colony formation assay. U2OS cells were seeded sparsely in 6 well plates, at 100 cells/well for low doses or 200 cells/well for high doses of damage. Cells were given 8-24 hours to adhere and then irradiated with UV. Cells were grown until the untreated group formed colonies of approximately 50 cells in density, which, depending on the doubling time of the cell line, took between 10 and 14 days. To visualize colonies, cells were washed once with ice-cold PBS and then fixed in 3% crystal violet in methanol for 15 min. Crystal violet was removed by gently submerging plates in water. Visible colonies were then quantified with Bantex colony counter 920A.

Cell and protein lysate treatments. Cells were treated with 10 Gy of IR for 4 hours using X-Ray 320 irradiator (Precision X-Ray Inc., N. Brandford, CT). The following drug treatments were used to treat cells: 5 mM Camptothecin (CPT; Sigma # C9911) for 4 hours; 1 μM Shield-1 (Takara # 632189) for 4 hours; 1 μM or 500 nM 4-Hydroxytamoxifen (4-OHT; Sigma # H7904) for 4 hours to induce Fok1- or AsiSI-dependent DSB, respectively. Protein lysates for DNA-RNA hybrid pull-down assays were treated with 10 μL RNaseA (Sigma # R6148) or with 10 μL RNaseH (NEB # M0297S) for 30 min at 37ºC.

Antibodies. Primary antibodies used for western blotting, immunoprecipitation (IP) and immunofluorescence (IF) are as follows: HELZ (ThermoFisher customized 1:50 for western; Proteintech # 26635-1-AP; 1:1000 for western, 1.2 mL per 1 mg DNA for CHIP, 1:1000 for PLA);

S9.6 (Millipore #MABE1095; 1:600 for Slot Blot, 1:250 for IF, 0.5 mL per one million cell nuclei for DRIP-WB, 5U per 1 mg DNA for DRIP) ; ssDNA (Millipore #MAB3868; 1:1000 for Slot Blot); IgG (Invitrogen # 10500C and Sigma # N103 for CHIP); GFP (Santa Cruz Tech # SC996; 1:1000 for western; and abcam # ab290; 1:5000 for western, 1 mg per 2 mg lysate for IP); γH2AX (Cell Signaling Technology # 2577S; 1:500 for IF; and Millipore # 05-636; 1:6000 for IF); KU80 (abcam # 80592; 1:1000 for western); GAPDH (Santa Cruz tech # sc-47724; 1:1000 for western); 53BP1 (Bethyl # A300-273A; 1:1000 for IF); RPA32 (Santa Cruz Tech # sc-14692; 1:400 for western); pRPA32 S4/8 (Bethyl # A700-009; 1:1000 for western); RPA70 (Cell Signaling # 2267S; 1:120 for IF); CtIP (Millipore # MABE1060; 1:1000 for western); γH2AX (Millipore # 05-636; 1:6000 for IF); γH2AX (Active Motif # 39117; 1 mL per 1 mg DNA for CHIP); Senataxin (Novus biological # NB100-57542; 1:1000 for IF) Rad51 (abcam # ab176458; 1:1000 for IF); Lamin A/C (Cell Signaling #2032; 1:1000 for western) RFP (abcam # ab125244; 1:1000 for western). Secondary antibodies used for western (at 1:1000) are: donkey anti-rabbit IR Dye 800 (Licor Biosciences #926-32213); donkey anti-rabbit IR Dye 680 (Licor Biosciences # 926-68023); donkey anti-mouse IR Dye 800 (Licor Biosciences # 926-32213); donkey anti-mouse IR Dye 680 (Licor Biosciences # 926-68022). Secondary antibodies used for IF (at 1:1000) are: goat anti-mouse Alexa Fluor 555 (Invitrogen # A21424); goat anti-rabbit Alexa Fluor 488 (Invitrogen # A11034); goat anti-mouse Alexa Fluor 647 (Invitrogen # A21235).

Plasmids, siRNA and sgRNA. Plasmids expressing full length GFP-HELZ were generated by cloning HELZ into the BamH1 and EcoR1 restriction sites of pcDNA3.1-GFP (Addgene # 70219) and RFP (Addgene # 13032), respectively (done by Emory Integrated Genomics Core). The plasmid was used to purify HELZ and as template for the construction of GFP-HELZ K674N by

QuickChange site-directed mutagenesis (Agilent) for rescue assays. RNaseH1-mCherry was purchased (Addgene #60365 and #60367).

The following siRNAs were used: HELZ-2 (CAGCACACCUUGUUAAAUC; Dharmacon # D-021180-02); HELZ-3 (GAUAUCACGUGGAAGACUU; Dharmacon # D-021180-03); HELZ-4 (CUACAGAAGAUCUCGAAUA; Dharmacon # D-021180-04); HELZ-UTR (GGAAAUAGAACGCAUCAAA; Dharmacon #D-021180-01) ATR (GAACAACACUGCUGGUUUG; Dharmacon # D-003202-05); BRCA2 (GAGACACAAUUACAACUAAA); CTIP (GAGCAGACCUUUCUCAGUA; Dharmacon # D-011376-01); sgHELZ (GATACTTTGGCTGGACGACTGG; Sigma # HS0000373232).

Transfections. For plasmid transfections, 1-4 million cells were seeded on 60 mm plates and 24 hours post plating, cells were transfected with 2-5 µg of the indicated plasmid using Lipofectamine 3000 as per manufacturer's instructions (ThermoFisher). Transfection medium was exchanged to fresh medium and cells were moved to 10 cm plates 4- 6 hours post-transfection. Cells were harvested 2-4 days post-transfection for downstream assays.

RNAi silencing. HELZ was silenced using RNAi Max reagent using the protocol outlined by the manufacturer (Invitrogen). In brief, 30-60 nmol siRNA was transfected into one million cells in 60 mm plates. Medium was exchanged to fresh medium 24 hours post transfection and grown for additional 24-48 hours as needed for subsequent assays.

Protein lysate, fractionation and western blotting. Harvested cells were washed in PBS buffer and then lysed for 30 min on ice in Nonidet P-40 buffer (200 mM NaCl, 1% Nonidet P-40, 50 mM Tris·HCl pH 8.0) freshly supplemented with protease inhibitors. Lysates were clarified by centrifugation (15,700×g, 10 min at 4 °C), and the supernatants were then collected. Protein concentration was determined by Bradford and resolved by SDS/PAGE, transferred onto PVDF, and probed using the desired primary antibodies. Signal was detected using the Li-Cor Odyssey system. Separation of U2OS cellular compartments was performed according to the manufacturer's instructions with a Standard Cell Fractionation kit (abcam # ab109719). Two different markers were used to assess the purity of each fraction: cytoplasm (GAPDH) and nucleus (Lamin A/C).

Immunoprecipitation. Protein lysate prepared as described above (750 µg for an over-expressed protein) was precleared with 30 µL of protein G or protein A agarose beads (Roche # 10042392 and Invitrogen # 15918-014, respectively) for one hour. Precleared lysate was added to 30 µL protein G or A agarose beads that were prebound to the IP antibody and incubated overnight on a rotator at 4ºC. Beads were washed three time with 0.375% CHAPS buffer on a rotator at room temperature and then resuspended in 50/50 0.375% CHAPS buffer and 5X SDS buffer. Resuspended beads were boiled for 10 min at 100ºC, centrifuged and supernatant was processed for western blotting as indicated.

DNA-RNA hybrid Immunoprecipitation-Western Blot (DRIP-WB). DRIP-WB assay was performed using Magna Nuclear RIP™ (Native) RNA-Binding Protein Immunoprecipitation Kit (Millipore/Sigma # 17-10522) following the manufacturer's recommended procedure with

modifications. Briefly, same number of cells were counted from each condition to prepare nuclear lysate. The nuclei resuspended in RIP lysis buffer was passed 2X through an insulin syringe, snap-frozen on dry ice. Next, the nuclear lysate was thawed at 37°C and centrifuged at 10,000 x g for 10 min at 4°C. 100 µL from this final nuclear lysate was incubated and rotated overnight at 4°C with 10 µl of magnetic beads resuspended with either S9.6 or IgG antibody. For RNase A or RNase H digestion, the lysate was incubated 30 min at 37°C prior to addition of magnetic beads. Next day, beads were separated placing on magnetic separator for 1 min. Supernatant was discarded and beads were washed twice for 20 min on rotor at 4°C with ice cold Nuclear RIP Wash buffer. The DNA-RNA hybrid was eluted by re-suspending the magnetic beads in 5X SDS-PAGE loading buffer followed by 10 min boiling at 100°C. Supernatant was processed for western blotting as described above.

DR-GFP assay. U20S DR-GFP cells were transfected with the siRNA of interest. Twenty-four hours later, medium was removed, and cells were transfected with 3 µg I-SceI and 2 µg of either the empty RFP plasmid or the indicated SAMHD1-RFP rescue plasmid. Seventy-two hours later, cells were harvested, washed twice with PBS, resuspended in PBS and subjected to flow cytometry (Aurora Cytek) for GFP and RFP fluorescence. To measure HR efficiency, percentage of GFP positive cells (HR positive) within the RFP positive cells (ie. Those transfected with empty or rescue plasmids) was analyzed using the FlowJo software.

Immunofluorescence. Appropriate number of U2OS cells were transfected with the indicated siRNA and seeded on coverslips. Overexpression with plasmids were performed 24 hours later if mentioned for the particular experiment. Treatment with IR or drug was done 4 hours prior to

fixation. For U20S-265 mCherry-LacI-Fok1 cells, treatment with 1 µM Shield-1 and 1 µM 4-OHT was done for 4 hours to induce recombinant Fok1 expression. 72 hours after siRNA, the coverslips were washed with PBS, fixed in 4% paraformaldehyde for 20 min at room temperature and permeabilized with 0.5% Triton X-100 for 10 min on ice. Blocking with 5% BSA was done for 1 hour following with overnight incubation with the indicated primary antibodies at 4°C. For RNase H (NEB # M0297S) or RNase A (Sigma #R6148) treatment, cells were treated for 30-60 min at 37°C before fixation with RNase A (40 µg in 500 µl Phosphate buffer saline (PBS). Secondary antibody staining was performed for 1 hour. DNA was stained with DAPI and coverslips were mounted on slides. Immunofluorescence signals were visualized using a 63x oil objective on a Zeiss Observer Z1 microscope equipped with Axiovision Rel 4.8 software. DNA-RNA hybrid immune-detection was conducted as described[61]. Briefly, coverslips of attached U2OS cells were washed with PBS and fixed with ice-cold 100% methanol for 10 min at -20°C, followed by 1 min incubation with cold acetone at room temperature. Coverslips were then washed three times with SSC 4X buffer and blocked in 4X SSC+3% BSA for 1 hour. Primary antibody S9.6 (1:250) was incubated overnight at 4°C. The subsequent steps were as described above. Enzymatic treatments with RNase H or RNase A were performed after methanol/acetone fixation for 30 min at 37C in PBS and then rinsed in SCC 4X twice before blocking.

Proximity Ligation Assay (PLA). PLA experiments were performed using the DuoLink In Situ Red Starter Kit Mouse/Rabbit (Millipore/Sigma-Aldrich # DUO92101-1KT) and following manufacturer protocol. U2OS cells were knocked down for the gene of interest, seeded on coverslips and treated with etoposide after 72 hours for 4 hours if indicated. For HELZ or

γH2AX/S9.6 PLA, coverslips containing U2OS cells were processed following the DNA-RNA hybrid immune-detection described above.

DNA-RNA hybrid immunodetection by slot blot. Cells were harvested after 72 hours siRNA knockdown with or without 4 hours etoposide treatment and genomic DNA was isolated with DNeasy Blood and Tissue kit (Qiagen # 69504). Nucleic acid was measured by nanodrop, 0.5 µg DNA was used from each condition. DNA was treated with 0.5 N NaOH and 1.5 M NaCl for 10 min to denature the DNA and neutralized for another 10 min in 0.5 M Tris-HCl buffer (pH 7.0) containing 1 M NaCl. RNase H treatment was done on the same amount of DNA followed by 1 hour incubation at 37°C. All samples were then brought up to a final volume of 200 µl with 20X SSC buffer and blotted onto presoaked Nitrocellulose membrane in 20X SSC buffer using a slot blot apparatus (Whatman Schleicher & Schuell Minifold I). After UV-cross linking (0.12 J/m2), we blocked in 5% BSA. Next, the non-treated and RNase H treated part of the membrane were subjected to blotting with S9.6 while the treated membrane serving as loading control was stained with single-stranded DNA antibody.

Micronuclei assay. Cells were knock downed for HELZ and seeded on coverslips. In the next 48 hours, cells were treated with 3 µg/ml cytochalasin B or left untreated for 12 hours, prior to fixation at 72 hours post knockdown. Cells were fixed in 4% paraformaldehyde, stained with DAPI, mounted on coverslips and imaged. Percent of binucleated cells with one or more DAPI positive micronucleus were quantified. 300 binucleated cells were counted per group.

Cell cycle analysis. Cells were knocked down for the gene of interest. 72 hours later, they were harvested, washed and resuspended in cold PBS followed by fixation with cold 70% ethanol on ice for a minimum of 1 hour. After washing twice in PBS, cells were treated with RNase A and stained with propidium iodide at room temperature for a minimum of 30 min. Finally, at least 25,000 cells were analyzed for propidium iodide fluorescence on a flow cytometer (Cytek Aurora). Debris and aggregates were excluded throughout analysis by FlowJo software.

ChIP assay. ChIP assay was performed using ChromaFlash™ One-Step ChIP Kit (P-2025, Epigentek, Farmingdale, NY, USA) according to the manufacture's instruction. Briefly, DIvA cells were treated with Shield-1 and 4-OHT for 4 hours to induce DSBs, then fixed with 1% formaldehyde (Sigma-252549) for 15 min at room temperature. After two washes with cold PBS, 0.125 M glycine was added for 5 min to quench formaldehyde reaction. Next, the cells were washed twice with PBS lysed by 0.75% CHAPS in lysis buffer (10% glycerol, 150 nM NaCl, 50 nM Tris pH-7.5). The lysed cells were sonicated to an average size of 500-800 base pairs using a Branson microtip SFX250 sonicator. Antibodies described above were used for immunoprecipitation for 4 hours at room temperature with IgG as the negative control. The obtained immunoprecipitated chromatin was subjected to quantitative real-time (PowerTrack™ SYBR Green Master Mix A46012, PCR 7500 Fast Real-Time PCR system, ThermoFisher) using primers specific for no-DSBs, HR1 and HR2 prone sites in DIvA cells.

	Forward primer	Reverse primer
no-DSBs	ATTGGGTATCTGCGTCTAGTGAGG	GACTCAATTACATCCCTGCAGCT
HR1	GATTGGCTATGGGTGTGGAC	CATCCTTGCAAACCAGTCCT
HR2	CCGCCAGAAAGTTTCCTAGA	CTCACCCTTGCAGCACTTG

DNA-RNA hybrid Immunoprecipitation-sequencing (DRIP-seq).

Genomic DNA was extracted from ~2 million U2OS cells transfected with siNC or siHELZ and fragmented with restriction enzymes (BsrGI, EcoRI, HindIII, SspI, XbaI, 30 U/each, NEB) following a published protocol [62]. Fragmented nucleic acids were recovered by phenol-chloroform extraction. Four ug of fragmented gDNA was digested with 20 U of RNase H (NEB #M0297S) at 37°C for 6 hours to serve as a negative control. Four ug of fragmented gDNA or RNase H digested DNA were immunoprecipitated with 8 µg of S9.6 antibody (Millipore #MABE1095) overnight at 4°C in DRIP binding buffer (10 mM sodium phosphate, 140 mM sodium chloride, 0.05% (v/v) Triton-X-100, pH 7.0). DNA-antibody complex was then incubated with 40 µL of Protein G beads (Invitrogen #10003D) for 2 hours at 4°C, and beads were washed three times with DRIP binding buffer. Antibody-captured DNA-RNA hybrids were then eluted in (50 mM Tris, 10 mM EDTA, 0.5% (v/v) SDS, pH 8.0) at 55°C for 45 min and subjected to phenol-chloroform extraction. The immunoprecipitated DNA-RNA hybrids were quantified by Qubit (ThermoFisher Scientific #Q32854). Ten ng of DNA-RNA hybrids were treated with 5 U of RNase H for 1 hour and then were sonicated into small fragments (~100-500 bp) using a Covaris Focused-Ultrasonicator Me220. Fragmented DNA was blunted, 5′ phosphorylated and 3’ A-tailed by NEBNext Ultra II End Prep Enzyme Mix following the manufacturer’s instruction (New England Biolabs #E7645L). An adaptor was ligated, and USER enzyme was used for U excision to yield adaptor ligated double-strand DNA. The DNA was then PCR-amplified using barcoded PCR primers (New England Biolabs #E7335L, #E7500L). After AMPure XP bead purification (Beckman Coulter #A63881) and Qubit quantification, the libraries were sent to Admera Health for quality analysis and sequencing. Equimolar pooling of libraries was performed, and 8-12 samples were pooled in one lane. Libraries were sequenced on a HiSeq with a read length configuration of 150 PE, targeting 740 M total reads per lane (370 M in each direction).

Bioinformatic analysis for DRIP-seq

DRIP-seq reads were aligned to the human genome sequence (hg38) by Bowtie2 version 2.4.4 with default parameter [63]. Aligned reads in the bam file were sorted by genomic coordinate by SAMtools [64] . Peaks for each library were identified by MACS2 version 2.2.6 compared to their corresponding input bam file [65]. DRIP-seq peaks identified from siNT and siHELZ were merged and reads were re-counted in the merged peak regions. Differential analysis was conducted by DESeq2 based on the reads count matrix in the merged peak regions and significantly changed regions were defined by FDR<0.05 [66]. The differential regions were annotated to genes by annotatePeaks.pl from HOMER version 4.11 [67].

Data availability

Data are available upon reasonable request from the authors.

Acknowledgements

We thank Dr. Roger Greenberg for U20S-235 mCherry-LacI-Fok1 cells, Dr. Jeremy Stark for U20S-DR-GFP cells, and Dr. Gaelle Legube for AsiSI-ER-U2OS cells. We thank members of the Yu lab for their helpful discussion and technical expertise. This work was supported by: National Institutes of Health (NIH) National Cancer Institute (NCI) [R01CA178999, R01CA254403, and U54CA274513 to D.S.Y.]. Research reported in this publication was supported in part by the Emory Integrated Genomics Core (EIGC) Shared Resource of Winship Cancer Institute of Emory University and NIH/NCI under award number P30CA138292. The content is solely the responsibility of the authors and does not necessarily represent the official views of the NIH.

Author Contributions

R.H., A.E.K., and D.S.Y. conceived and designed the study. R.H., A.E.K., M.Z.M., S.R., Y.H., and B.Y.S. performed and analyzed the experiments. R.H., A.E.K., S.K.R., M.Z.M., Y.H., B.S.S., A.M.K., L.L., B.Y., and D.S.Y. interpreted the findings. R.H. and D.S.Y. wrote the manuscript with input from all authors.

Competing interests

The authors declare no competing interests.

Figure legends

Figure 1. HELZ depletion causes hypersensitivity to DSB-inducing agents and HELZ localizes and binds to DSBs. a-b HELZ depletion causes hypersensitivity to etoposide (**a**) and IR (**b**). U2OS cells were transfected with indicated siRNA. 96 hours (h) after transfection, cells were treated with or without indicated doses of etoposide or IR. Mean and standard deviation (SD) from three independent replicas is shown. **c** Western blot analysis showing HELZ knockdown in U2OS cells from **a**-**b**. **d** U2OS-265 Fok1 cells were transfected with GFP-HELZ, and induced for Fok1 expression with 1 μM Shield-1 and 1 μM 4-OHT for 4 hours. Samples were processed for direct immunofluorescence with mCherry-Fok1 and GFP-HELZ and indirect immunofluorescence with anti-γH2AX antibody. DNA was visualized by DAPI staining. **e** Representative images and **f** quantification from two independent replicas of PLA foci between HELZ and γH2AX before and after treatment with 20 μM etoposide for 4 hours. The median is indicated by a horizontal line. *** $p < 0.001$. **g-h** CHIP-qPCR analysis of endogenous HELZ enrichment at HR1 (**g**) and HR2 (**h**) prone DNA repair sites in DIvA cells. DSBs were induced by treatment with 500 nM 4-OHT for 4 hours. For **g-h,** mean and standard error of the mean (SEM) from three independent replicas is shown. * indicates $p < 0.05$, ** $p<0.01$, *** $p < 0.001$, ns indicates not significant.

Figure 2. HELZ depletion causes genomic instability via R loop accumulation. a-b U2OS cells were transfected with HELZ and NT siRNA and processed 72 hours later for indirect immunofluorescence for spontaneous γH2AX foci. Representative images and quantification are shown. **c-d** Micronuclei formation in U2OS cells 72 hours following HELZ depletion. Cells were fixed and stained with DAPI (**c**) and quantified (**d**). **e-f** Immunofluorescence staining for

spontaneous 53BP1 nuclear bodies was performed in U2OS cells depleted for HELZ or a NT control or in U2OS HELZ KO cells generated by CRISPR/Cas9. Representative images and quantification are shown. **g** Western blot showing KO of HELZ in U2OS cells. **h-i** Representative images and quantification for 53BP1 nuclear bodies in U2OS cells silenced for HELZ or a NT control and rescued for spontaneous 53BP1 nuclear bodies with overexpression of mCherry-RNaseH1. The median is indicated by a horizontal line. *** $p < 0.001$. For **b**, **d,** and **f**, mean and SD from three independent replicas is shown. ** $P<0.01$, *** $p < 0.001$.

Figure 3. HELZ prevents accumulation of R loops through its helicase activity. a-b U2OS cells were transfected with HELZ siRNA and processed 72 hours later for indirect immunofluorescence with anti-S9.6 antibody. Representative images (**a**) and quantification (**b**) are shown. The median is indicated by a horizontal line. *** $p < 0.001$. **c** Slot blot analysis of DNA-RNA hybrids from HCT116 cells transfected with indicated siRNA and cDNA with or without etoposide treatment. Equal amounts of DNA treated or untreated with RNase H (+) or denatured (ssDNA), were loaded as indicated. The membrane was immunoblotted with anti-S9.6 antibody or antibody recognizing ssDNA to verify equivalent DNA loading. **d** Western blot analysis showing HELZ knockdown and overexpression in HCT116 cells used in **c**. **e** DNA-RNA hybrid immunoprecipitation western blot (DRIP-WB) analysis of lysate from U2OS cells demonstrating pull-down of endogenous HELZ with and without treatment with etoposiode, CPT, RNase H, and RNase A for 30 min. **f** ChIP-qPCR analysis of endogenous HELZ and S9.6 enrichment at HR1 prone DNA repair site. DSBs were induced by treating DIvA cells with 500 nM of 4-OHT for 4 hours. Mean and SD from three independent replicas is shown. *** $p < 0.001$. **g-h** PLA foci

suggesting an interaction between γH2AX and S9.6 in U2OS cells 72 hours following HELZ knockdown. Representative images and quantification are shown. The median is indicated by a horizontal line. *** $p < 0.001$.

Figure 4. HELZ depletion causes global accumulation of R loops. a Ngsplot of R-loop read counts across all R-loop peaks identified in siNT and siHELZ cells. **b** Ngsplot of R-loop read counts across defined human RefSeq (hg38) genes. **c** Volcano plot showing the number of R-loop regions increased or decreased in HELZ depleted U2OS cells. The R-loop regions that achieved an FDR of <0.05 and fold-change of ≥2 are indicated in red (increased) and blue (decreased). **d** Ngsplot of R-loop read counts across the accumulated R-loop regions. **e** Ngsplot of R-loop read counts across the depleted R-loop regions. **f** Genomic distribution of significantly upregulated and downregulated R-loop regions.

Figure 5. HELZ promotes homologous recombination by preventing accumulation of R loops at DSBs. a U2OS cells transfected with indicated siRNA were seeded for colony formation. 72 hours post transfection, cells were treated with indicated doses of ABT888 every 2-3 days. Percent survival colonies is shown. **b** HEK293 cells containing an integrated DR-GFP HR reporter were silenced with indicated siRNA, and transfected with I-SceI endonuclease and RFP (-) or RFP-HELZ (WT, Mut K674N) as shown. Live cells collected were subjected to flow cytometry. RFP-expressing cell population was sorted and percent of GFP positive cells within this population was determined to analyze HR efficiency. **c** Western blot analysis showing HELZ knockdown and expression of RFP-HELZ WT and MUT from **b**. **d** c-NHEJ DNA repair efficacy in HEK293 cells integrated with the EJ-7 c-NHEJ reporter substrate and transfected with indicated siRNA and

Cas9/sgRNA.. **e** Western blot analysis showing HELZ knockdown from **d**. **f-g** U2OS cells were depleted for HELZ for 72h, treated with 4 Gy IR with or without RNase H or RNase A treatment for 1 hour, and processed 4h after IR for indirect immunofluorescence with indicated antibodies. Representative images and quantitation are shown. The median is indicated by a horizontal line. *** $p < 0.001$. **h-i** U2OS cells were depleted for HELZ for 72h, treated with 4 Gy IR, and processed 4h later for indirect immunofluorescence with indicated antibodies. Representative images and quantitation are shown. The median is indicated by a horizontal line. *** $p < 0.001$. For **a-b**, and **d**, mean and SD from three independent replicas is shown. * $p < 0.05$, *** $p < 0.001$.

References

1 Sanz, L. A. *et al.* Prevalent, Dynamic, and Conserved R-Loop Structures Associate with Specific Epigenomic Signatures in Mammals. *Molecular cell* **63**, 167-178, doi:10.1016/j.molcel.2016.05.032 (2016).

2 Garcia-Muse, T. & Aguilera, A. R Loops: From Physiological to Pathological Roles. *Cell* **179**, 604-618, doi:10.1016/j.cell.2019.08.055 (2019).

3 Petermann, E., Lan, L. & Zou, L. Sources, resolution and physiological relevance of R-loops and RNA-DNA hybrids. *Nature reviews. Molecular cell biology* **23**, 521-540, doi:10.1038/s41580-022-00474-x (2022).

4 Aguilera, A. & Gomez-Gonzalez, B. DNA-RNA hybrids: the risks of DNA breakage during transcription. *Nat Struct Mol Biol* **24**, 439-443, doi:10.1038/nsmb.3395 (2017).

5 Brickner, J. R., Garzon, J. L. & Cimprich, K. A. Walking a tightrope: The complex balancing act of R-loops in genome stability. *Molecular cell* **82**, 2267-2297, doi:10.1016/j.molcel.2022.04.014 (2022).

6 Crossley, M. P., Bocek, M. & Cimprich, K. A. R-Loops as Cellular Regulators and Genomic Threats. *Molecular cell* **73**, 398-411, doi:10.1016/j.molcel.2019.01.024 (2019).

7 Li, F. *et al.* R-Loops in Genome Instability and Cancer. *Cancers (Basel)* **15**, doi:10.3390/cancers15204986 (2023).

8 Niehrs, C. & Luke, B. Regulatory R-loops as facilitators of gene expression and genome stability. *Nature reviews. Molecular cell biology* **21**, 167-178, doi:10.1038/s41580-019-0206-3 (2020).

9 Richard, P. & Manley, J. L. R Loops and Links to Human Disease. *J Mol Biol* **429**, 3168-3180, doi:10.1016/j.jmb.2016.08.031 (2017).

10 Ciccia, A. & Elledge, S. J. The DNA damage response: making it safe to play with knives. *Molecular cell* **40**, 179-204, doi:10.1016/j.molcel.2010.09.019 (2010).

11 Jackson, S. P. & Bartek, J. The DNA-damage response in human biology and disease. *Nature* **461**, 1071-1078, doi:10.1038/nature08467 (2009).

12 Scully, R., Panday, A., Elango, R. & Willis, N. A. DNA double-strand break repair-pathway choice in somatic mammalian cells. *Nature reviews. Molecular cell biology* **20**, 698-714, doi:10.1038/s41580-019-0152-0 (2019).

13 Ouyang, J. *et al.* RNA transcripts stimulate homologous recombination by forming DR-loops. *Nature* **594**, 283-288, doi:10.1038/s41586-021-03538-8 (2021).

14 Wei, W. *et al.* A role for small RNAs in DNA double-strand break repair. *Cell* **149**, 101-112, doi:10.1016/j.cell.2012.03.002 (2012).

15 Marnef, A. & Legube, G. R-loops as Janus-faced modulators of DNA repair. *Nat Cell Biol* **23**, 305-313, doi:10.1038/s41556-021-00663-4 (2021).

16 Hasgall, P. A. *et al.* The putative RNA helicase HELZ promotes cell proliferation, translation initiation and ribosomal protein S6 phosphorylation. *PLoS One* **6**, e22107, doi:10.1371/journal.pone.0022107 (2011).

17 Hanet, A. *et al.* HELZ directly interacts with CCR4-NOT and causes decay of bound mRNAs. *Life Sci Alliance* **2**, doi:10.26508/lsa.201900405 (2019).

18 Shanbhag, N. M., Rafalska-Metcalf, I. U., Balane-Bolivar, C., Janicki, S. M. & Greenberg, R. A. ATM-dependent chromatin changes silence transcription in cis to DNA double-strand breaks. *Cell* **141**, 970-981, doi:10.1016/j.cell.2010.04.038 (2010).
19 Aymard, F. *et al.* Transcriptionally active chromatin recruits homologous recombination at DNA double-strand breaks. *Nat Struct Mol Biol* **21**, 366-374, doi:10.1038/nsmb.2796 (2014).
20 Wang, I. X. *et al.* Human proteins that interact with RNA/DNA hybrids. *Genome Res.* **28**, 1405-1414 (2018).
21 Pause, A. & Sonenberg, N. Mutational analysis of a DEAD box RNA helicase: the mammalian translation initiation factor eIF-4A. *EMBO J* **11**, 2643-2654, doi:10.1002/j.1460-2075.1992.tb05330.x (1992).
22 O'Sullivan Coyne, G. *et al.* PARP inhibitor applicability: detailed assays for homologous recombination repair pathway components. *Onco Targets Ther.*, 165-180 (2022).
23 Yang, X. *et al.* RNA-DNA hybrids regulate meiotic recombination. *Cell reports* **37**, 110097, doi:10.1016/j.celrep.2021.110097 (2021).
24 Alzu, A. *et al.* Senataxin associates with replication forks to protect fork integrity across RNA-polymerase-II-transcribed genes. *Cell* **151**, 835-846, doi:10.1016/j.cell.2012.09.041 (2012).
25 Mischo, H. E. *et al.* Yeast Sen1 helicase protects the genome from transcription-associated instability. *Molecular cell* **41**, 21-32, doi:10.1016/j.molcel.2010.12.007 (2011).
26 Skourti-Stathaki, K., Proudfoot, N. J. & Gromak, N. Human senataxin resolves RNA/DNA hybrids formed at transcriptional pause sites to promote Xrn2-dependent termination. *Molecular cell* **42**, 794-805, doi:10.1016/j.molcel.2011.04.026 (2011).
27 Sollier, J. *et al.* Transcription-coupled nucleotide excision repair factors promote R-loop-induced genome instability. *Molecular cell* **56**, 777-785, doi:10.1016/j.molcel.2014.10.020 (2014).
28 Ngo, G. H. P., Grimstead, J. W. & Baird, D. M. UPF1 promotes the formation of R loops to stimulate DNA double-strand break repair. *Nature communications* **12**, 3849, doi:10.1038/s41467-021-24201-w (2021).
29 Tran, P. L. T. *et al.* PIF1 family DNA helicases suppress R-loop mediated genome instability at tRNA genes. *Nature communications* **8**, 15025, doi:10.1038/ncomms15025 (2017).
30 Marabitti, V. *et al.* ATM pathway activation limits R-loop-associated genomic instability in Werner syndrome cells. *Nucleic acids research* **47**, 3485-3502, doi:10.1093/nar/gkz025 (2019).
31 Chang, E. Y. *et al.* RECQ-like helicases Sgs1 and BLM regulate R-loop-associated genome instability. *J Cell Biol* **216**, 3991-4005, doi:10.1083/jcb.201703168 (2017).
32 Bjorkman, A. *et al.* Human RTEL1 associates with Poldip3 to facilitate responses to replication stress and R-loop resolution. *Genes & development* **34**, 1065-1074, doi:10.1101/gad.330050.119 (2020).
33 Hodson, C. *et al.* Branchpoint translocation by fork remodelers as a general mechanism of R-loop removal. *Cell reports* **41**, 111749, doi:10.1016/j.celrep.2022.111749 (2022).

34 Lafuente-Barquero, J. *et al.* The Smc5/6 complex regulates the yeast Mph1 helicase at RNA-DNA hybrid-mediated DNA damage. *PLoS genetics* **13**, e1007136, doi:10.1371/journal.pgen.1007136 (2017).

35 Schwab, R. A. *et al.* The Fanconi Anemia Pathway Maintains Genome Stability by Coordinating Replication and Transcription. *Molecular cell* **60**, 351-361, doi:10.1016/j.molcel.2015.09.012 (2015).

36 Ozdemir, A. Y., Rusanov, T., Kent, T., Siddique, L. A. & Pomerantz, R. T. Polymerase theta-helicase efficiently unwinds DNA and RNA-DNA hybrids. *The Journal of biological chemistry* **293**, 5259-5269, doi:10.1074/jbc.RA117.000565 (2018).

37 Nguyen, D. T. *et al.* The chromatin remodelling factor ATRX suppresses R-loops in transcribed telomeric repeats. *EMBO reports* **18**, 914-928, doi:10.15252/embr.201643078 (2017).

38 Li, L. *et al.* DEAD Box 1 Facilitates Removal of RNA and Homologous Recombination at DNA Double-Strand Breaks. *Molecular and cellular biology* **36**, 2794-2810, doi:10.1128/MCB.00415-16 (2016).

39 Li, L., Monckton, E. A. & Godbout, R. A role for DEAD box 1 at DNA double-strand breaks. *Molecular and cellular biology* **28**, 6413-6425, doi:10.1128/MCB.01053-08 (2008).

40 Ribeiro de Almeida, C. *et al.* RNA Helicase DDX1 Converts RNA G-Quadruplex Structures into R-Loops to Promote IgH Class Switch Recombination. *Molecular cell* **70**, 650-662 e658, doi:10.1016/j.molcel.2018.04.001 (2018).

41 Mersaoui, S. Y. *et al.* Arginine methylation of the DDX5 helicase RGG/RG motif by PRMT5 regulates resolution of RNA:DNA hybrids. *EMBO J* **38**, e100986, doi:10.15252/embj.2018100986 (2019).

42 Bader, A. S. *et al.* DDX17 is required for efficient DSB repair at DNA:RNA hybrid deficient loci. *Nucleic acids research* **50**, 10487-10502, doi:10.1093/nar/gkac843 (2022).

43 Lin, W. L. *et al.* DDX18 prevents R-loop-induced DNA damage and genome instability via PARP-1. *Cell reports* **40**, 111089, doi:10.1016/j.celrep.2022.111089 (2022).

44 Hodroj, D. *et al.* An ATR-dependent function for the Ddx19 RNA helicase in nuclear R-loop metabolism. *EMBO J* **36**, 1182-1198, doi:10.15252/embj.201695131 (2017).

45 Argaud, D., Boulanger, M. C., Chignon, A., Mkannez, G. & Mathieu, P. Enhancer-mediated enrichment of interacting JMJD3-DDX21 to ENPP2 locus prevents R-loop formation and promotes transcription. *Nucleic acids research* **47**, 8424-8438, doi:10.1093/nar/gkz560 (2019).

46 Song, C., Hotz-Wagenblatt, A., Voit, R. & Grummt, I. SIRT7 and the DEAD-box helicase DDX21 cooperate to resolve genomic R loops and safeguard genome stability. *Genes & development* **31**, 1370-1381, doi:10.1101/gad.300624.117 (2017).

47 Perez-Calero, C. *et al.* UAP56/DDX39B is a major cotranscriptional RNA-DNA helicase that unwinds harmful R loops genome-wide. *Genes & development* **34**, 898-912, doi:10.1101/gad.336024.119 (2020).

48 Mosler, T. *et al.* R-loop proximity proteomics identifies a role of DDX41 in transcription-associated genomic instability. *Nature communications* **12**, 7314, doi:10.1038/s41467-021-27530-y (2021).

49 Weinreb, J. T. *et al.* Excessive R-loops trigger an inflammatory cascade leading to increased HSPC production. *Dev Cell* **56**, 627-640 e625, doi:10.1016/j.devcel.2021.02.006 (2021).

50 Marchena-Cruz, E. *et al.* DDX47, MeCP2, and other functionally heterogeneous factors protect cells from harmful R loops. *Cell reports* **42**, 112148, doi:10.1016/j.celrep.2023.112148 (2023).

51 Chakraborty, P. & Grosse, F. Human DHX9 helicase preferentially unwinds RNA-containing displacement loops (R-loops) and G-quadruplexes. *DNA repair* **10**, 654-665, doi:10.1016/j.dnarep.2011.04.013 (2011).

52 Chakraborty, P. & Hiom, K. DHX9-dependent recruitment of BRCA1 to RNA promotes DNA end resection in homologous recombination. *Nature communications* **12**, 4126, doi:10.1038/s41467-021-24341-z (2021).

53 Chakraborty, P., Huang, J. T. J. & Hiom, K. DHX9 helicase promotes R-loop formation in cells with impaired RNA splicing. *Nature communications* **9**, 4346, doi:10.1038/s41467-018-06677-1 (2018).

54 Cristini, A., Groh, M., Kristiansen, M. S. & Gromak, N. RNA/DNA Hybrid Interactome Identifies DXH9 as a Molecular Player in Transcriptional Termination and R-Loop-Associated DNA Damage. *Cell reports* **23**, 1891-1905, doi:10.1016/j.celrep.2018.04.025 (2018).

55 Cohen, S. *et al.* Senataxin resolves RNA:DNA hybrids forming at DNA double-strand breaks to prevent translocations. *Nature communications* **9**, 533, doi:10.1038/s41467-018-02894-w (2018).

56 Yuce, O. & West, S. C. Senataxin, defective in the neurodegenerative disorder ataxia with oculomotor apraxia 2, lies at the interface of transcription and the DNA damage response. *Molecular and cellular biology* **33**, 406-417, doi:10.1128/MCB.01195-12 (2013).

57 Sakasai, R. *et al.* Aquarius is required for proper CtIP expression and homologous recombination repair. *Sci Rep* **7**, 13808, doi:10.1038/s41598-017-13695-4 (2017).

58 Cohen, S. *et al.* A POLD3/BLM dependent pathway handles DSBs in transcribed chromatin upon excessive RNA:DNA hybrid accumulation. *Nature communications* **13**, 2012, doi:10.1038/s41467-022-29629-2 (2022).

59 Matsui, M. *et al.* USP42 enhances homologous recombination repair by promoting R-loop resolution with a DNA-RNA helicase DHX9. *Oncogenesis* **9**, 60, doi:10.1038/s41389-020-00244-4 (2020).

60 Sessa, G. *et al.* BRCA2 promotes DNA-RNA hybrid resolution by DDX5 helicase at DNA breaks to facilitate their repairdouble dagger. *EMBO J* **40**, e106018, doi:10.15252/embj.2020106018 (2021).

61 Renaudin, X., Lee, M., Shehata, M., Surmann, E.-M. & Venkitaraman, A. R. BRCA2 deficiency reveals that oxidative stress impairs RNaseH1 function to cripple mitochondrial DNA maintenance. *Cell Rep.* **36**, 109478 (2021).

62 Sanz, L. A. & Chedin, F. High-resolution, strand-specific R-loop mapping via S9.6-based DNA-RNA immunoprecipitation and high-throughput sequencing. *Nat Protoc* **14**, 1734-1755, doi:10.1038/s41596-019-0159-1 (2019).

63 Langmead, B. & Salzberg, S. L. Fast gapped-read alignment with Bowtie 2. *Nature Methods* **9**, 357-359, doi:10.1038/nmeth.1923 (2012).

64 Li, H. *et al.* The Sequence Alignment/Map format and SAMtools. *Bioinformatics* **25**, 2078-2079, doi:10.1093/bioinformatics/btp352 (2009).

65 Zhang, Y. *et al.* Model-based Analysis of ChIP-Seq (MACS). *Genome Biology* **9**, R137, doi:10.1186/gb-2008-9-9-r137 (2008).

66 Love, M. I., Huber, W. & Anders, S. Moderated estimation of fold change and dispersion for RNA-seq data with DESeq2. *Genome Biology* **15**, doi:10.1186/s13059-014-0550-8 (2014).

67 Duttke, S. H., Chang, M. W., Heinz, S. & Benner, C. Identification and dynamic quantification of regulatory elements using total RNA. *Genome Research* **29**, 1836-1846, doi:10.1101/gr.253492.119 (2019).

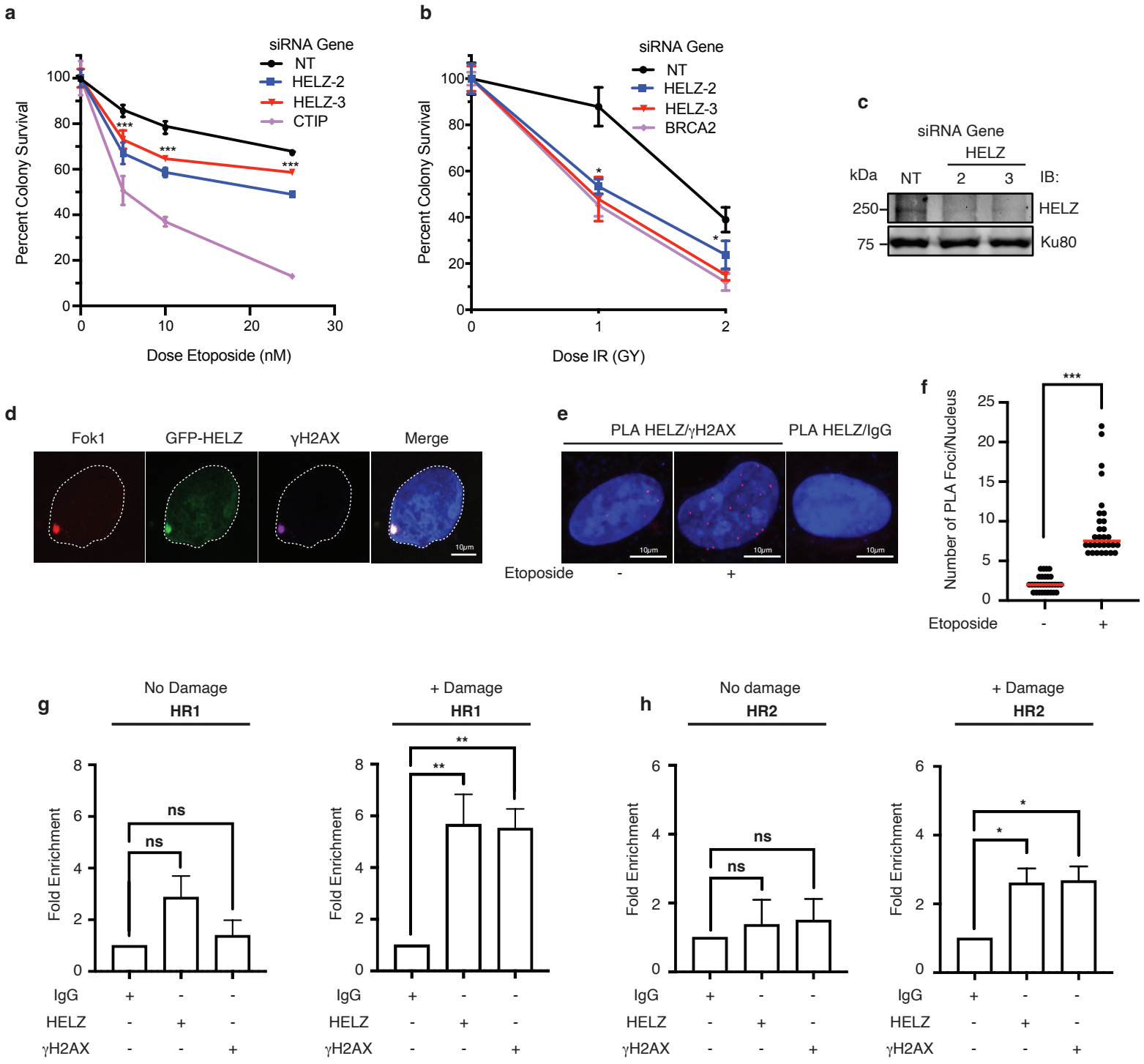

Figure 1- HELZ depletion causes hypersensitivity to DSB-inducing agents and HELZ localizes and binds to DSBs.

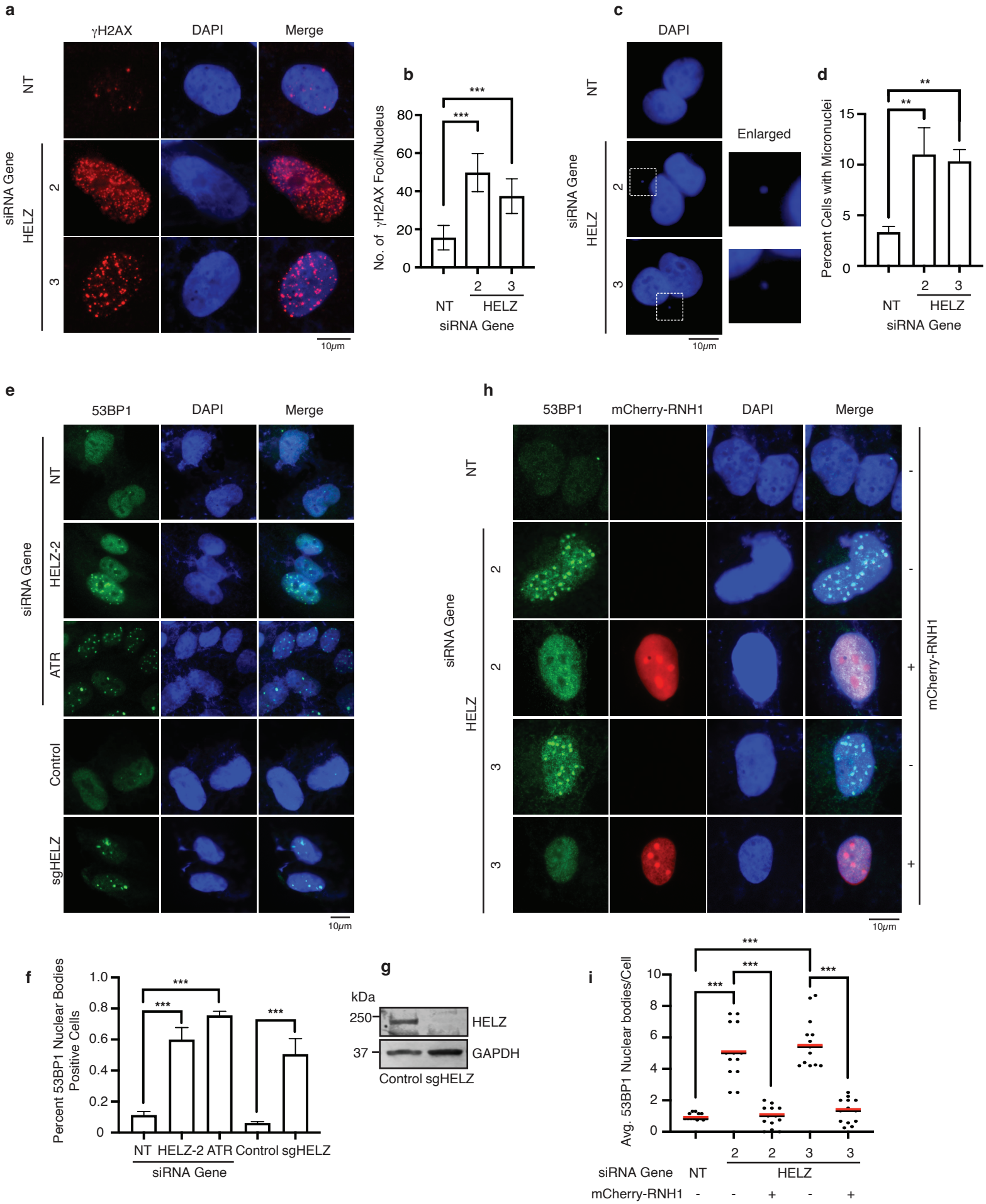

Figure 2- HELZ depletion causes genomic instability via R loop accumulation.

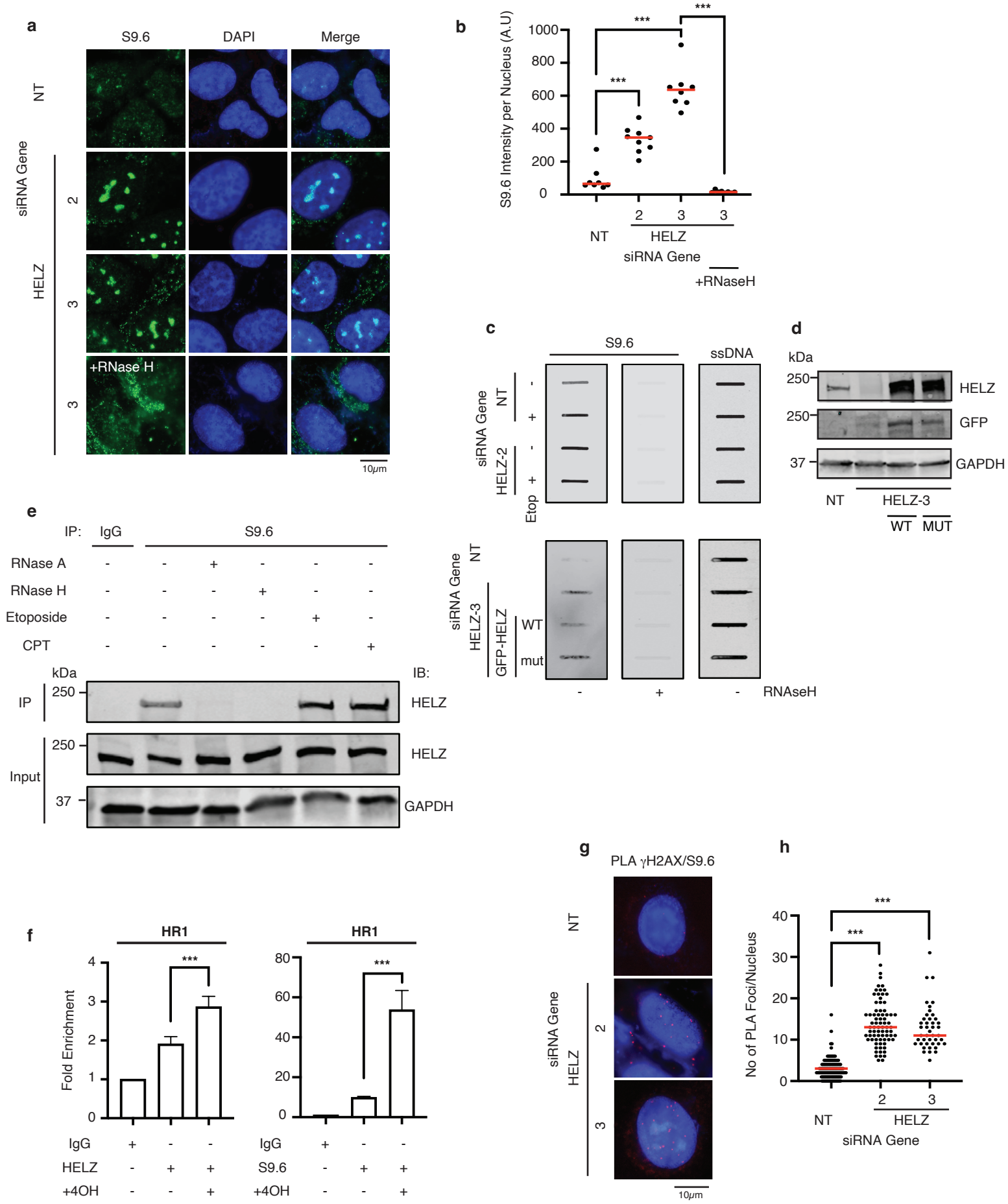

Figure 3- HELZ prevents accumulation of R loops through its helicase activity.

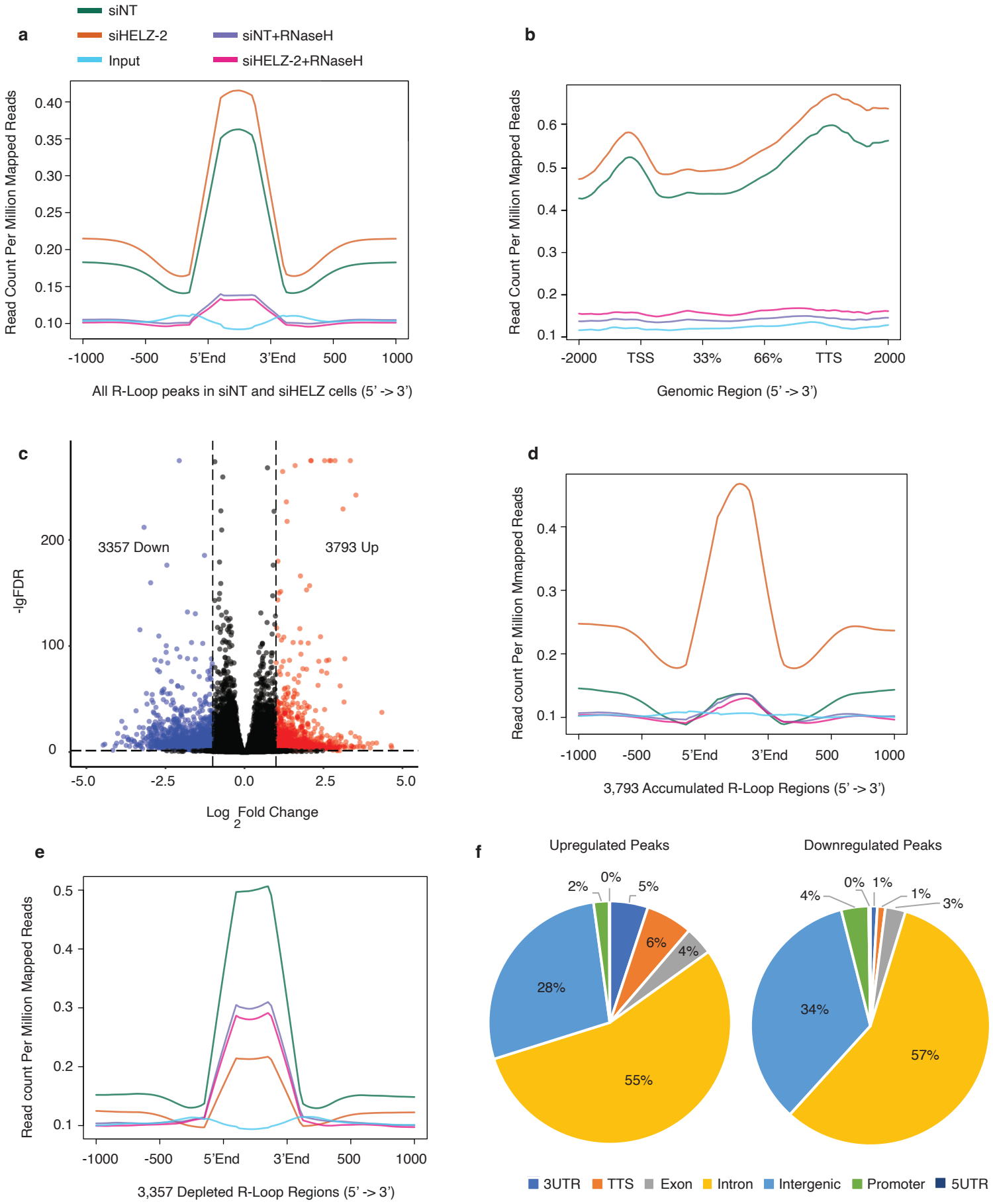

Figure 4- HELZ depletion causes global accumulation of R loops.

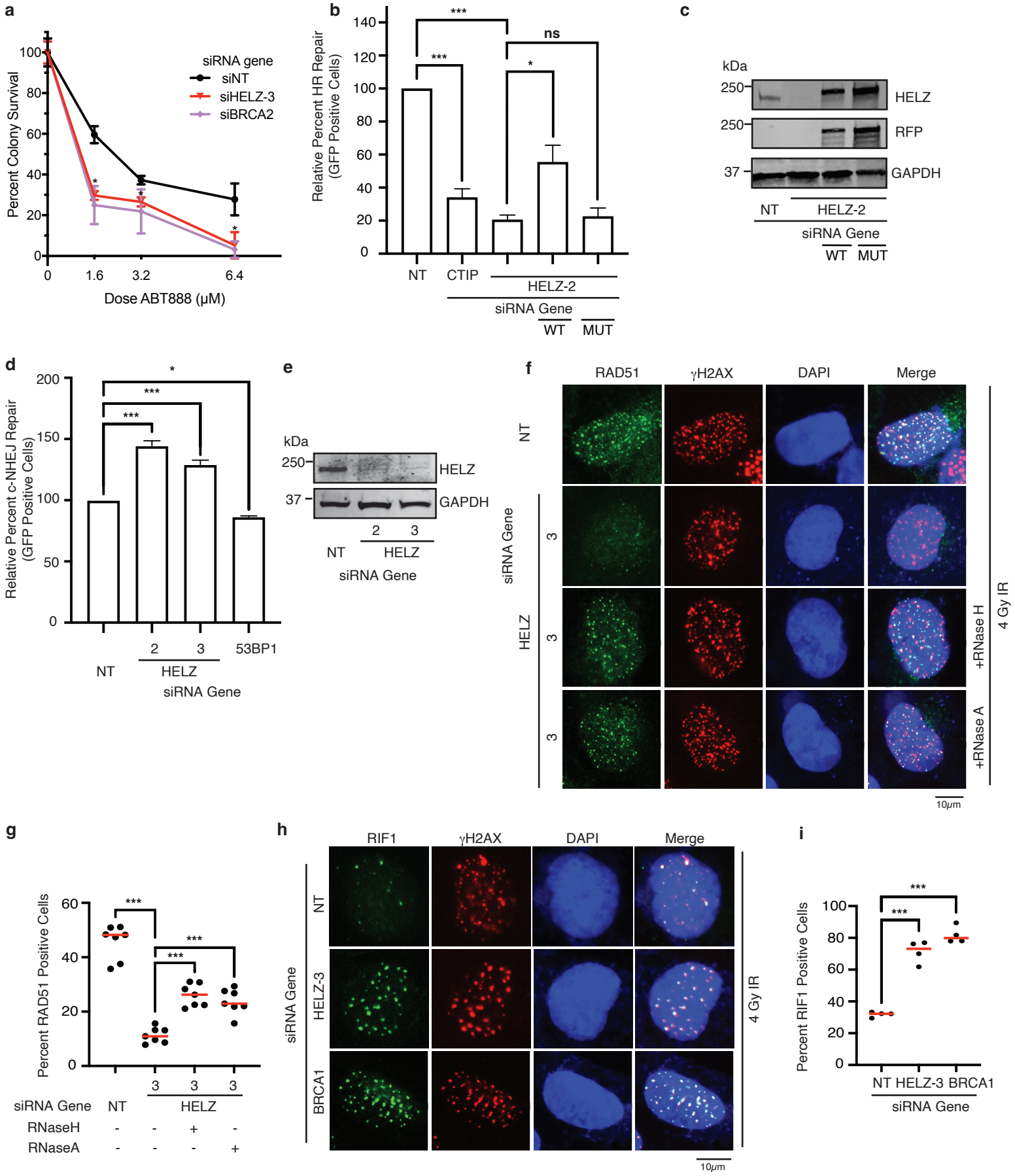

Figure 5- HELZ promotes homologous recombination by preventing accumulation of R loops at DSBs.